Wetting in fcc Ising antiferromagnets and binary alloys. II. A Monte Carlo and renormalization-group study

G. Gompper
Sektion Physik der Ludwig-Maximilians-Universität München, 8000 München 2, West Germany

D. M. Kroll
Institut für Festkörperforschung, KFA Jülich, Postfach 1913, 5170 Jülich, West Germany
(Received 23 November 1987; revised manuscript received 11 January 1988)

The order-disorder transition at the surface of an fcc Ising antiferromagnet with nearest- and next-nearest-neighbor interactions which exhibits an $L1_2$ (A_3B) ground-state structure is studied using Monte Carlo and renormalization-group methods. Monte Carlo results for the surface phase diagram, critical behavior of both excess and local quantities, as well as the short-range-order parameter at the surface are presented. The critical behavior is shown to be consistent with the predictions of mean-field theory.

I. INTRODUCTION

The nature of wetting transitions in systems with short-ranged interactions in $d=3$ dimensions is still rather controversial.[1,2] In particular, computer simulations of critical wetting in the three-dimensional (3D) Ising model have yielded results which are consistent with simple mean-field behavior;[3] the rather exotic critical singularities predicted by various renormalization-group treatments[4-8] were not observed. This discrepancy between theory and simulation data is one of the central open questions in the field of interfacial critical phenomena.

Direct experimental tests of the theory would therefore be very useful. This may be possible in a semi-infinite magnetic insulator (in which the interactions are short ranged) with a bulk first-order phase transition. In this case, a narrow region of high-temperature disordered phase can intervene at the free surface and finally wet it at the bulk transition temperature, T^*, where the ordered and the disordered phases coexist.[9] When this occurs, the order at the surface goes continuously to zero and low-energy electron-diffraction (LEED), spin-polarized LEED (SPLEED), or total-reflection experiments using synchrotron radiation or neutrons can be used to determine the wetting critical behavior.

In order to provide some guidance for such experiments, we have studied surface-induced disorder (SID) transitions in an fcc Ising antiferromagnet with nearest- and next-nearest-neighbor interactions which exhibits an $L1_2$ (A_3B) ground-state structure. The model is general enough to illustrate several generic features of wetting in ordering alloys and magnets with short range interactions. In particular, more than one density is needed to describe the ordered state; this makes it possible to study the influence of surface segregation and was shown in Ref. 10 to lead to qualitative new nonuniversal wetting behavior.

In the first paper of this series[10] we investigated this model using the mean-field (MF) approximation. In the present paper we extend our analysis to include fluctuation effects. The outline of the paper is as follows: The essential features of the MF analysis are reviewed in Sec. II. The wetting behavior at (100) and (111) surfaces is described and an interface displacement model, in which the dynamic variable is the local distance of the interface between the ordered bulk and the disordered surface phases and the crystal surface, is introduced. This model is then studied using functional renormalization-group (RG) methods in Sec. III. Our Monte Carlo (MC) results for the 3D lattice model are described in Sec. IV. The surface phase diagram, critical behavior of both excess and local surface quantities, as well as the behavior of the short-range-order parameter at the surface are described. The critical behavior is shown to be consistent with simple MF behavior. Section V contains a brief summary and concluding remarks.

II. FROM THE ISING ANTIFERROMAGNET TO THE EFFECTIVE INTERFACE MODEL

Our analysis is based on a lattice-gas model for binary alloys. At each site of a fcc lattice there is a spin variable $s_i=\pm 1$. We assume an interaction Hamiltonian of the form

$$\mathcal{H}=J\sum_{(\mathrm{NN})}s_is_j-\alpha J\sum_{(\mathrm{NNN})}s_is_j-HJ\sum_i s_i - H_1J\sum_{\substack{i \text{ in} \\ \text{first layer}}}s_i-H_2J\sum_{\substack{i \text{ in} \\ \text{second layer}}}s_i\ , \tag{2.1}$$

where the first sum ranges over nearest-neighbor (NN) and the second over next-nearest-neighbor (NNN) pairs of sites. We take $\alpha>0$ so that $J>0$ and $\alpha J>0$ correspond to antiferromagnetic NN interactions and ferromagnetic NNN interactions, respectively. The other terms in (2.1) describe the effect of bulk and surface magnetic fields. We do not consider modified surface coupling constants here.

This model has been used extensively to study ordering fcc alloys (such as the Cu-Au system).[11,12] The isomorphism between (2.1) and a lattice-gas model for binary alloys is defined by the variable transformation $c_i=(1+s_i)/2$. In this way a concentration variable $c_i=1$ (0) can be identified with an A (B) atom at each site of the lattice. In the present paper we formulate our treatment in terms of the Ising Hamiltonian (2.1).

In the MF approximation one finds that continuous wetting transitions occur for appropriately chosen surface fields as the A_3B bulk order-disorder transition is crossed going from the ordered to the disordered state.[13–16] The wetting behavior depends on the crystallographic orientation of the surface:[10] while the order at the surface vanishes with an exponent $\beta_1=\frac{1}{2}$ at the (111) surface, β_1 is nonuniversal at (100) surfaces. In particular, its value depends on the relative strength of the NN and NNN interactions: we obtain $\beta_1=2.22$ for $\alpha=0.2$, and $\beta_1=2.8$ for $\alpha=0.1$ in the MF approximation in this case.

The reason for the drastic difference in behavior at these two surfaces is that while one length scale (measured for example by the width of the MF order parameter interface) dominates in the [111] direction, there are two characteristic lengths of comparable size in the [100] direction. It is the competition between these two length scales which leads to the nonuniversal behavior. This effect is rather easy to understand in terms of an interface displacement model. The dynamical variable in this model, z, is the local distance of the interface from the free surface. The free-energy functional, which is derived in Ref. 10, has the form

$$F\{z\}=\sigma_f+A_1e^{-\lambda_1 z}+B_1e^{-2\lambda_1 z}$$

$$+A_2e^{-\lambda_2 z}+B_2e^{-2\lambda_2 z}+\cdots+tz\ , \qquad (2.2)$$

where $t=(T^*-T)/T^*$ is the reduced temperature and λ_1,λ_2 are the inverse correlation lengths of the order parameter (OP) and the magnetization in the disordered (surface) phase. σ_f is the surface tension of the free interface. The temperature dependence of the coefficients $A_1,\ldots,B_2$ is negligible near the transition. A_1 is proportional to a staggered field in the surface; it is identically zero for model (2.1).

In order to characterize the wetting behavior, two cases need to be distinguished.[10,17,18]

(i) $\lambda_2>2\lambda_1$: The leading exponential term is $e^{-2\lambda_1 z}$, and the resulting critical behavior is the same as in the single-order-parameter case. The order parameter at the surface, $\eta_1=\partial F/\partial A_1\mid_{A_1=0}$, vanishes at t^{β_1} with $\beta_1=\frac{1}{2}$. At tricriticality, where $B_1=0$ in this case, we obtain $\beta_1'=\lambda_1/\lambda_2$ for $\lambda_2<3\lambda_1$, and $\beta_1'=\frac{1}{3}$ for $\lambda_2>3\lambda_1$.

(ii) $\lambda_2<2\lambda_1$: The term $e^{-\lambda_2 z}$ determines the wetting behavior, so that $\beta_1=\lambda_1/\lambda_2$. At tricriticality, where $A_2=0$ in this case, we obtain $\beta_1'=\lambda_1/(2\lambda_2)$ for $\lambda_1>\lambda_2$, and $\beta_1'=\frac{1}{2}$ for $\lambda_1<\lambda_2<2\lambda_1$.

For a (111) surface $\lambda_2\gg\lambda_1$. The critical behavior is therefore the same as in the single-order-parameter case. On the other hand, for the (100) surface the MF analysis of the lattice model with $\alpha=0.2$ yields $\lambda_1=1.6266$ and $\lambda_2=0.7335$, so that $\lambda_2<\lambda_1$ (which implies $\lambda_2<2\lambda_1$); we thus find $\beta_1=2.22$ and $\beta_1'=\beta_1/2$.

The surface magnetization also exhibits a singular temperature dependence.[1] Since the coefficients B_1, A_2, $B_2,\ldots$, in (2.2) are linear in H_1, one has

$$\delta m_1(t):=m_1(t)-m_1(0)=\text{const}\times\langle e^{-2\lambda_1 z}\rangle$$

$$+\text{const}\times\langle e^{-\lambda_2 z}\rangle+\cdots\ .$$

This implies

$$\delta m_1(t)=a_1t+a_2t^{3/2}+\cdots+a_\lambda t^{\lambda_2/2\lambda_1}+\cdots$$

for the (111) surface ($\lambda_2\gg\lambda_1$), and

$$\delta m_1(t)=b_1t+b_2t^2+\cdots+b_\lambda t^{2\lambda_1/\lambda_2}+\cdots$$

for the (100) surface, where the a's and b's are constants.

III. RENORMALIZATION-GROUP THEORY

The renormalization-group treatment of the effective interface model for a single order parameter predicts a critical wetting behavior in $d=3$ which differs dramatically from the MF result. The critical exponents are found to depend continuously on the dimensionless parameter $\omega=k_BT\lambda^2/(4\pi\sigma)$, where σ is the stiffness of the free interface. In particular, the OP at the surface, η_1, vanishes as

$$\eta_1\sim t^{\beta}1\times[\ln(1/t)]^{\Psi}\ ,$$

where $\beta_1=(1+\omega)/2$, $\Psi=0$ for $\omega<\frac{1}{2}$; $\beta_1=\sqrt{2\omega}-\omega/2$, $\Psi=\sqrt{\omega/8}$ for $\frac{1}{2}<\omega<2$; and $\beta_1=1$, $\Psi=0$ for $\omega>2$ (Refs. 5, 6, 19, 20). This behavior is expected to be found at the (111) surface.

In order to determine the RG predictions for the critical behavior at the (100) surface, we follow the treatment of Fisher and Huse[6] for the single-order-parameter case.[21] For an arbitrary bare interface potential $V_0(z)$, the renormalized potential is given to linear order in V by

$$V_l(z)=\frac{e^{2l}}{\sqrt{4\pi\omega l}}\int_{-\infty}^{\infty}dz'V_0(z')e^{-(z-z')^2/(4\omega l)}\ , \qquad (3.1)$$

where l is the logarithm of the spatial rescaling factor. The critical behavior is determined by renormalizing the potential until its curvature at its minimum at $z=z_m$ is of order one and monotonically increasing. This occurs at the scale $\exp(l^*)$ given by $\partial^2 V_l^*/\partial z^2 \mid_{z_m} \cong 1$.

The average position of the interface, $\langle z \rangle$, will be given by the position z_m^* of the minimum of the renormalized potential at scale l^*; since there is no rescaling of perpendicular distances, $\langle z \rangle = z_m^*$.

For $\lambda_2 < 2\lambda_1$ [which is the relevant parameter range for $Cu_3Au(100)$], λ_2 sets the scale for z and defines ω. The surface OP is given by $\eta_1 \sim \langle \exp(-\lambda_1 z) \rangle$. Consider first the case $\lambda_1 > \lambda_2$. β_1 is determined from

$$\eta_1 \sim \left\langle \exp\left[-\frac{\lambda_1}{\lambda_2} z\right] \right\rangle = e^{2l^*} \frac{\partial V_{R,l^*}}{\partial A_1}\bigg|_{A_1=0} = \frac{1}{(4\pi\omega l^*)^{1/2}} \int_0^\infty dz' e^{-z'\lambda_1/\lambda_2} e^{-(z_m^*-z')^2/(4\omega l^*)} , \quad (3.2)$$

where z is now measured in units of λ_2^{-1}. For technical reasons, we define $z=\mu l$. The exponent in the integral (3.2) is maximized at $\mu' = \mu - 2\omega\lambda_1/\lambda_2$. For $\mu > 2\omega\lambda_1/\lambda_2$, the integral is therefore dominated by the saddle point, so that

$$\frac{1}{(4\pi\omega l^*)^{1/2}} \int_0^\infty d\mu' \exp\{l^*[-\mu'\lambda_1/\lambda_2 - (\mu-\mu')^2/(4\omega)]\} \sim \exp[-\mu l^* \lambda_1/\lambda_2 + \omega l^* (\lambda_1/\lambda_2)^2] . \quad (3.3)$$

From the RG treatment in Ref. 6 we know that for $\omega < 2$ we have

$$\mu l^* = z_m^* = -\frac{2+\omega}{2} \ln(t) , \quad (3.4a)$$

$$l^* \cong -\tfrac{1}{2}\ln(t) . \quad (3.4b)$$

Collecting everything together, we arrive at

$$\beta_1 = \frac{\lambda_1}{\lambda_2}\left[1 + \frac{\omega}{2}\left[1 - \frac{\lambda_1}{\lambda_2}\right]\right], \quad \Psi = 0 . \quad (3.5)$$

This result is correct as long as

$$2+\omega = \mu > 2\omega\lambda_1/\lambda_2 ,$$

i.e., for

$$\omega < (\lambda_1/\lambda_2 - \tfrac{1}{2})^{-1} =: \omega_1^* .$$

For $\mu < 2\omega\lambda_1/\lambda_2$ the integral is dominated by μ' near zero, so that

$$\frac{1}{\sqrt{4\pi\omega l^*}} \int_0^\infty d\mu' \exp\{l^*[-\mu'\lambda_1/\lambda_2 - (\mu-\mu')^2/(4\omega)]\} \sim \exp[-\mu^2 l^*/(4\omega) - \tfrac{1}{2}\ln(l^*)] , \quad (3.6)$$

from which we obtain

$$\beta_1 = \frac{(2+\omega)^2}{8\omega}, \quad \Psi = -\tfrac{1}{2} . \quad (3.7)$$

This result is valid for $\omega_1^* < \omega < 2$. Finally, for $\omega > 2$ we have

$$\langle z \rangle = -\sqrt{2\omega}\left\{\ln(t) + \tfrac{1}{4}\ln\left[\ln\left[\frac{1}{t}\right]\right]\right\} \quad (3.8)$$

instead of (3.4a). Together with (3.4b), we find from (3.6)

$$\beta_1 = 1, \quad \Psi = 0 . \quad (3.9)$$

For $\lambda_2 < 2\lambda_1 < 2\lambda_2$, $\omega_1^* > 2$. In this case, β_1 and Ψ are given by (3.5) for $\omega < 2$. For $2 < \omega < \omega_2^*$, with $\omega_2^* = 2(\lambda_2/\lambda_1)^2$, we have

$$\beta_1 = \frac{\lambda_1}{2\lambda_2}\left[\sqrt{8\omega} - \frac{\lambda_1}{\lambda_2}\omega\right], \quad \Psi = \frac{\lambda_1}{\lambda_2}\sqrt{\omega/8} . \quad (3.10)$$

Finally, for $\omega > \omega_2^*$ we again obtain the result (3.9).

Note that β_1 is a continuous function of ω which decreases monotonically with increasing ω for $\lambda_1 > \lambda_2$ and increases with increasing ω for $\lambda_2 < 2\lambda_1 < 2\lambda_2$.

The results for the tricritical exponents β_1^t and Ψ_t are given in Table I. β_1^t is a continuous function of ω. It decreases monotonically with increasing ω for $\lambda_1 > 2\lambda_2$, while it increases with increasing ω for $2\lambda_2 > \lambda_1 > \lambda_2/2$.

TABLE I. RG predictions for the tricritical exponents β_1^t and Ψ_t as a function $\omega=k_B T\lambda_2^2/(4\pi\sigma)$, for $2\lambda_1>\lambda_2$.

$\lambda_1>2\lambda_2$	$2\lambda_2>\lambda_1>\lambda_2$	$2\lambda_2>2\lambda_1>\lambda_2$
	$\beta_1^t=\frac{\lambda_1}{2\lambda_2}\left[1+\omega\left[2-\frac{\lambda_1}{\lambda_2}\right]\right]$, $\Psi_t=0$	$\beta_1^t=\frac{1+\omega}{2}$, $\Psi_t=0$
for $\omega<\frac{1}{2}(\lambda_1/\lambda_2-1)^{-1}\equiv\omega_{1,t}^*$	for $\omega<\frac{1}{2}$	for $\frac{1}{2}<\omega$
$\beta_1^t=\frac{(1+2\omega)^2}{8\omega}$, $\Psi_t=-\frac{1}{2}$	$\beta_1^t=\frac{\lambda_1}{2\lambda_2}\left[\sqrt{8\omega}-\frac{\lambda_1}{\lambda_2}\omega\right]$, $\Psi_t=\frac{\lambda_1}{\lambda_2}\sqrt{\omega/8}$	$\beta_1^t=\sqrt{2\omega}-\omega/2$, $\Psi_t=\sqrt{\omega/8}$
for $\omega_{1,t}^*<\omega<\frac{1}{2}$	for $\frac{1}{2}<\omega<\omega_2^*\equiv 2(\lambda_2/\lambda_1)^2$	for $\frac{1}{2}<\omega<2$
	$\beta_1^t=1$, $\Psi_t=0$	
for $\frac{1}{2}<\omega$	for $\omega_2^*<\omega$	for $2<\omega$

IV. MONTE CARLO SIMULATIONS

The Monte Carlo method has been used extensively to study the order-disorder phase transitions of the Ising model (2.1) in the bulk.[12,22,23] It is quite clear that the nearest-neighbor model ($\alpha=0$) cannot provide a good description of binary alloys, such as the CuAu system, even at stoichiometric compositions. Also, the next-nearest-neighbor model is at best a crude approximation. Nevertheless, the experimental long-range-order data for Cu_3Au at $c_{Au}=0.25$ and $c_{Au}=0.28$, are reproduced rather well for $\alpha=0.2$.[12] Therefore, we have chosen this value of α for most of our simulations; some data were also taken for $\alpha=0.1$ in order to check the α dependence of the wetting behavior.

We have confined our calculations to systems which are at stoichiometric A_3B composition in the bulk. Since we use the grand canonical ensemble, the chemical potentials μ_A and μ_B or, equivalently, the field H, are therefore a function of temperature. This temperature dependence of H, determined in a system with periodic boundary conditions, is shown in Fig. 1.

In the present simulations we consider a system of D (100) or (111) lattice planes, with periodic boundary conditions within the planes. For the (100) planes we measure the system size in units of the unit cell of the sc lattice—with the lattice constant a_0 being half of the next-nearest-neighbor distance in the fcc lattice—in which half of the lattice sites are occupied. In the (111) planes the B (Au) sites form a triangular net, which is generated by two primitive vectors $\mathbf{a}_1$ and $\mathbf{a}_2$ (with $|\mathbf{a}_1|=|\mathbf{a}_2|=2\sqrt{2}a_0$ and $\mathbf{a}_1\cdot\mathbf{a}_2=4a_0^2$). The system size in the (111) planes is then measured in units of $\mathbf{c}_1=\mathbf{a}_1/2$ and $\mathbf{c}_2=(\mathbf{a}_2-\mathbf{a}_1/2)/2$, so that $\mathbf{c}_1\cdot\mathbf{c}_2=0$. In both cases we have chosen as $L\times L$ geometry in the planes. Each (100) plane consists of $N=L^2/2$ spins, and each (111) plane of $N=L^2$ spins. The ordered structure fits the periodic boundary conditions only if L is even in case of the (100) planes, while for the (111) planes L has to be a multiple of 4. In order to keep the system size as small as possible, we take only one of the two boundary planes to be a free surface; effective bulk fields are introduced (in addition to H) at the other surface in order to simulate a semi-infinite system. It turns out that both magnetic and staggered fields are necessary in order to keep the concentration and the order parameter at their bulk values. These effective fields are also used to break the symmetry between the four equivalent ground states of the A_3B structure. For the (100) case, the surface is forced to be of the AB type (A type) by choosing of an even (odd) D and effective bulk fields which favor a pure A "bulk" plane.

A necessary condition for the MC study of the SID transition is that the "bulk" part of our system stays in a (metastable) ordered state. We find that this requires larger and larger lattices when coexistence between ordered and disordered phase is approach. This is the reason for our choice of lattice sizes (as well as for the introduction of the effective bulk fields, see the preceding), which vary from $L=12$ and $D=20$ to $L=50$ and $D=50$. Sampling techniques with preferential surface site selec-

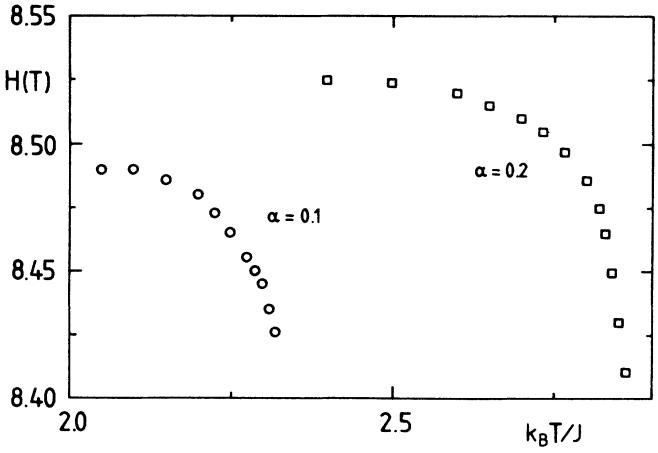

FIG. 1. Temperature dependence of the magnetic field H required to keep the bulk system at the stoichiometric A_3B composition. The fields for two different coupling constant ratios α are shown.

tion were used so that surface spins are flipped 10 times more often than bulk spins. After "equilibrium" was reached, typically 7500–50 000 MC steps per surface site were used for calculating the averages.

Since the critical surface behavior is expected to depend on the crystallographic direction of the surface, we present and discuss the results of the MC simulations for the (100) and the (111) surface separately.

A. (100) surface

The temperature variation of the OP in the first and the third layer is shown for two different surface fields in Fig. 2 for the case of an AB type surface. If not stated otherwise, all the following simulation data are obtained for this surface type. The surface transition can be either first or second order, depending on the choice of H_1 and H_2. From Fig. 2 we estimate the transition temperature to be $k_B T^*/J = 2.870 \pm 0.010$. This is in good agreement with the temperature of the order-disorder transition determined in MC simulations of the bulk system.[23]

1. Surface phase diagram

The first aim of our computer experiment is to determine the surface phase diagram: which surface fields lead to continuous surface transitions, and for which H_1, H_2 is the transition first order. The position of the boundary line between these two regions is most easily found by a variation of the surface fields at coexistence ($T = T^*$). Figure 3 shows the H_1 dependence of the surface OP η_1 for several fixed ratios H_2/H_1. For $H_2/H_1 > 0$, η_1 is found to vanish continuously with H_1. On the other hand, for $H_2/H_1 \leq 0$, $\eta_1(H_1)$ seems to behave discontinuously near $H_1 = -2.6$; increasing H_1 beyond the values shown in Fig. 3 leads to a complete disordering of the whole system.

The phase diagram, which is obtained from the data in Fig. 3, is shown in Fig. 4. The solid line which terminates at point 0 in Fig. 4 is a tricritical line. It

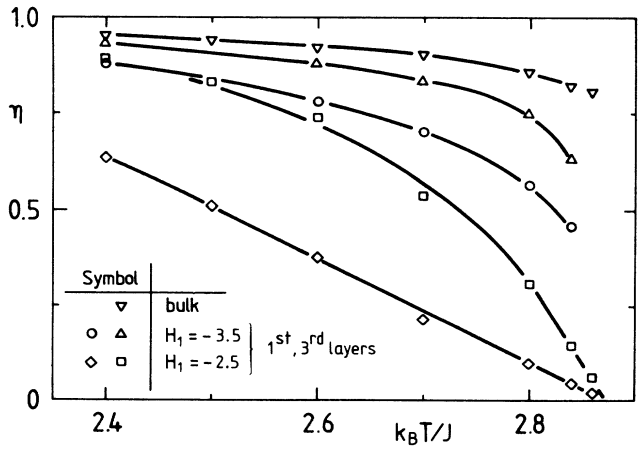

FIG. 2. Order parameter in the first and third layers at a (100) surface for surface fields $H_1 = -2.5$, $H_2 = -0.12$ ($\diamond$,$\square$), and $H_1 = -3.5$, $H_2 = +0.17$ ($\circ$,$\triangle$), as well as the bulk order parameter (∇), as a function of temperature T.

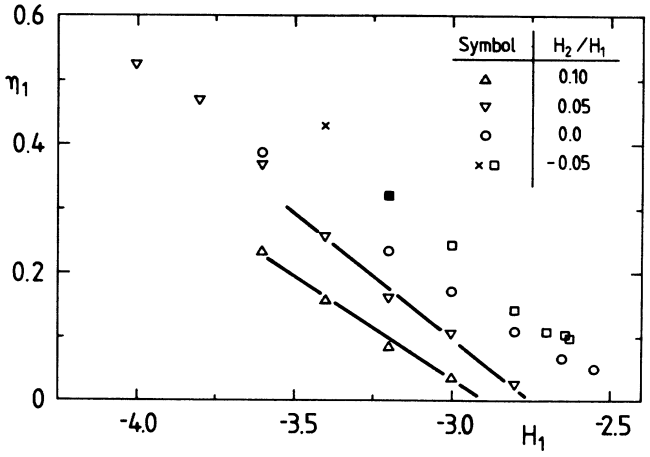

FIG. 3. Surface order parameter η_1 at coexistence ($T = 2.870$), as a function of the surface field H_1 and for several values of H_2/H_1; lattice size $L = 40$, $D = 46$. Some data shown [marked by crosses ($\times$)] are taken for $k_B T/J = 2.873$ with $L = 30$, $D = 38$.

separates the region of first order transitions (which occur for more negative values of H_1) from the region of continuous transitions. In terms of the interface displacement model (2.2), this line corresponds to $A_2 = 0$, $B_2 > 0$.[24] To the left of this line A_2 is negative, to the right it is positive. In the scenario we describe here, B_2 changes sign at the multicritical point 0.[25] For larger values of H_2, B_2 is negative. The dashed line is a line of first-order transitions; A_2 is positive along this line. A

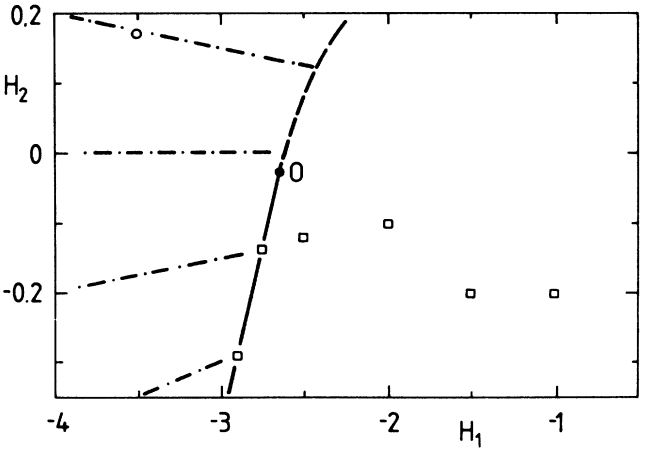

FIG. 4. Surface phase diagram for the AB-type surface in the (H_1, H_2) plane. The solid line is a line of tricritical transitions which separates the regions of continuous and discontinuous surface transitions; it is determined by linear interpolation between the data points. The dashed line indicates the approximate position of a line of first-order transitions. The dashed-dotted lines are the lines of constant H_2/H_1, along which $\eta_1(H_1)$ was measured as shown in Fig. 3. The squares (continuous transition) and the circle (discontinuous transition) indicate the values of surface fields for which we have determined the temperature dependence of several surface quantities, as discussed in the text.

sheet of prewetting transitions (not shown here) is expected to project out from this first-order line into the $t>0$ region of the full (t, H_1, H_2) phase diagram.

It can be seen that the H_2 dependence of the tricritical line is weak. A similar H_1 dependence of η_1 has been found in MF approximation. Even the value of the tricritical point $H_1^t=-2.70$ (calculated for $H_2=-0.2$ in the lattice MF treatment[10]) is in astonishing good agreement with the MC result $H_1^t=-2.81$ (obtained by a linear interpolation in Fig. 4). Since the concentration of A atoms increases with increasing H_1, Fig. 4 shows that a SID transition occurs if the A component is enriched at the surface.

The behavior of η_1 at coexistence as a function of surface field for the case of B segregation at the surface, i.e., for large negative values of H_1, is shown in Fig. 5. Of course, the surface OP decreases if the surface composition deviates from the ideal AB composition—in either direction. However, Fig. 5 shows that the surface order vanishes exponentially as $H_1\to-\infty$, i.e., with increasing B concentration in the surface. In contrast, we find that the OP in the third layer does not decrease substantially in this limit. The exponential decay of η_1 with large negative H_1 is therefore just the behavior of an antiferromagnet with a fixed staggered field (from the third layer) in an external magnetic field. Neither an interface delocalization transition nor a disordering transition in the surface occurs in this case.

These observations can be understood as follows: Due to the antiferromagnetic coupling, a B-rich surface leads to a high A concentration in the second layer. Then, in the third layer, which is the second layer of the AB type, an atom on an A site feels the existence of the free surface only through a single (ferromagnetic) next-nearest-neighbor coupling. If we assume that all layers further away from the surface are in their ordered bulk state, the next-nearest-neighbor interactions from the first and the fifth layer cancel each other at the A sites of the third layer; however, they favor the occupation of B sites by B atoms. Therefore, it is plausible that B segregation causes much less disorder in the neighboring layers than A segregation.

Finally, we want to demonstrate that a SID transition is also possible for the A-type surface. Figure 6 shows the H_1 dependence of η_1 at coexistence for this surface type. The relation between η_1 and H_1 in the region of incomplete SID is again almost linear. A linear extrapolation yields $(H_1^t, H_2^t)=(-2.66, -0.27)$ for the tricritical point. However, compared to the AB-type surface, the role of A and B segregation is reversed in this case: SID occurs only for large negative values of H_1, i.e., for high B concentrations in the surface. The heuristic argument given above for the AB-type surface can easily be modified to explain this behavior. Note that there is only a very small interval of surface fields where SID transitions are possible for both surface types.

2. *Critical surface behavior*

Next we turn to the investigation of the critical properties of various surface and excess quantities. We obtain the surface excess OP, η_s, from the OP profile as follows:

$$\eta_s=\sum_{\substack{n=1\\ n\ \text{odd}}}^{D-1}(\eta_b-\eta_n)\ , \tag{4.1}$$

where η_b is also calculated from the profile by

$$\eta_b=\tfrac{1}{4}\sum_{\substack{n=D-11\\ n\ \text{odd}}}^{D-5}\eta_n\ . \tag{4.2}$$

This definition of η_b does not coincide with the usual definition of the bulk OP in A_3B binary alloys,[22] since only the AB-type layers are taken into account here.

To calculate the surface excess susceptibility

$$\chi_s=\partial\eta_s/\partial h\,|_{h=0}\ , \tag{4.3}$$

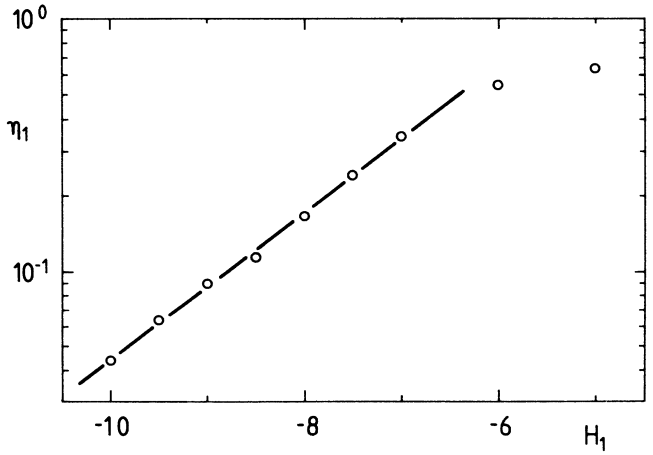

FIG. 5. Surface order parameter η_1 near coexistence ($k_BT/J=2.860$) as a function of the surface field H_1, for large negative H_1, with $H_2/H_1=0.1$ and $L=40$, $D=46$.

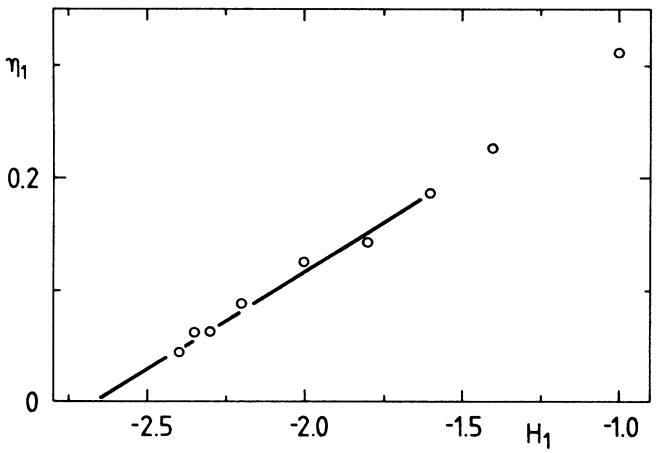

FIG. 6. Surface order parameter η_1 for the A-type surface (η_1 is here the OP of the second layer), at coexistence ($k_BT/J=2.870$) as a function of the surface field H_1, for $H_2/H_1=0.1$ and $L=40$, $D=45$.

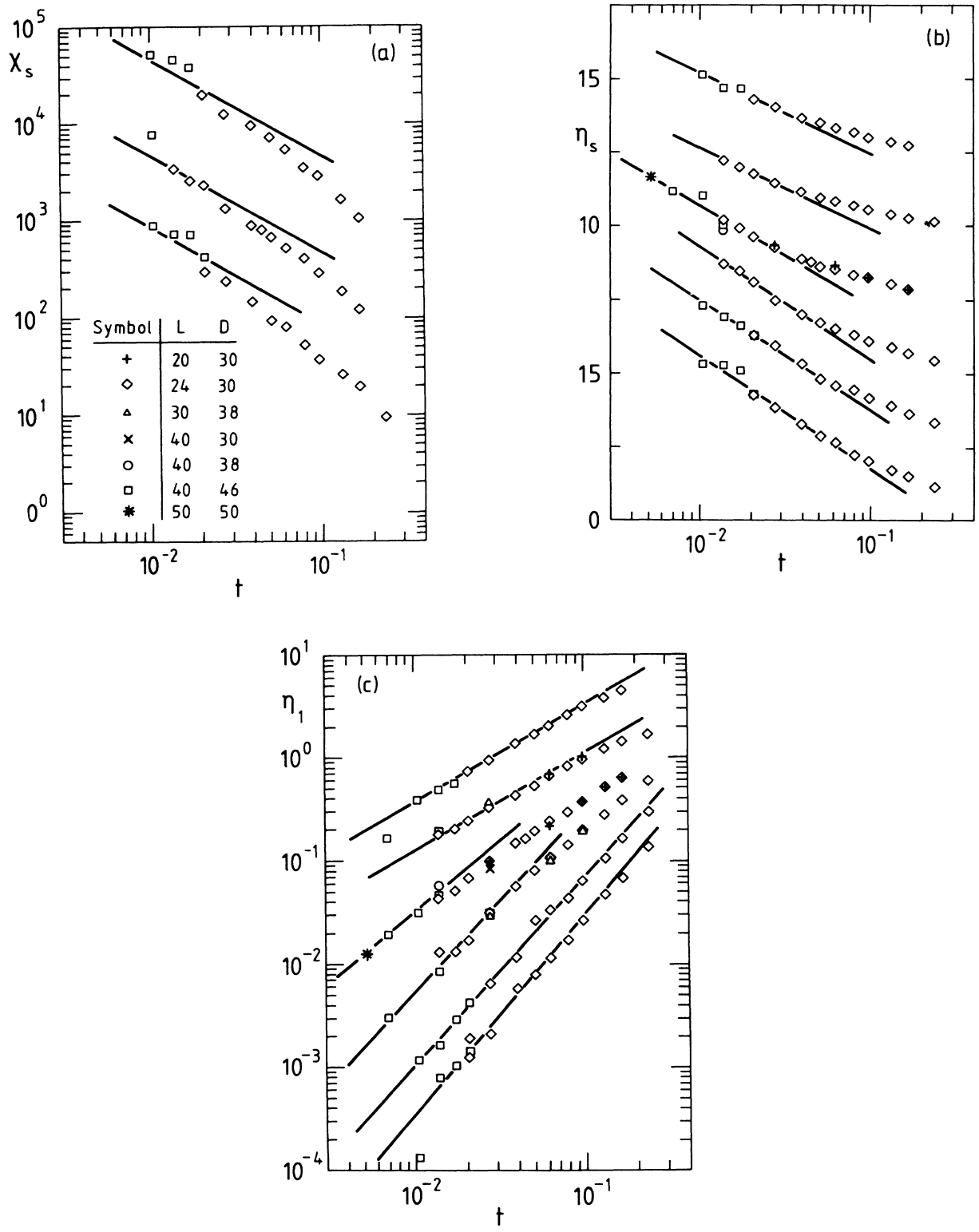

FIG. 7. Surface excess susceptibility χ_s (a), surface excess order parameter η_s (b), and surface order parameter η_1 (c) for the (100) surface, plotted as a function of the reduced temperature t (with $k_B T^*/J = 2.880$) for several values of the surface fields (Ref. 26). In (a), data shown are (from bottom to top) for $H_1 = -1.0$, $H_2 = -0.2$, for $H_1 = -2.5$, $H_2 = -0.12$, and for $H_1 = -2.9$, $H_2 = -0.29$. Data for successive values of the fields are multiplied by a factor of 10 to separate them in the figure. In (b) and (c), data shown are (from bottom to top) for $H_1 = -1.0$, $H_2 = -0.2$, for $H_1 = -1.5$, $H_2 = -0.2$, for $H_1 = -2.0$, $H_2 = -0.1$, for $H_1 = -2.5$, $H_2 = -0.12$, for $H_1 = -2.75$, $H_2 = -0.1375$, and for $H_1 = -2.9$, $H_2 = -0.29$. In (b), data for succcessive values of the fields are incremented by 2.5 to separate them in the figure. In (c), the data for $H_1 = -2.75$ and $H_1 = -2.9$ are multiplied by a factor of 2 and 6, respectively. The solid lines are an approximate fit to the asymptotic slope of the data.

where h is the (staggered) field conjugate to η, we use the fluctuation-dissipation relation

$$k_B T \chi_s = N \left[\left\langle \sum_i (\eta_b - \eta_i) \sum_j (\eta_b - \eta_j) \right\rangle - \eta_s^2 \right] . \quad (4.4)$$

The temperature dependence of the η_s and χ_s are shown as a function of the reduced temperature $t = (T^* - T)/T^*$ for several surface fields in Figs. 7(a) and 7(b).[26] Both MF and RG theory predict the following critical behavior:

$$\eta_s \sim -\ln(t) , \qquad \chi_s \sim t^{-1} . \quad (4.5)$$

The MC data show the predicted scaling behavior. It is nice to see that the deviations from scaling occur in both η_s and χ_s at about the same value of $t \cong 0.05$.

For a more detailed comparison between MF theory and MC results, we show lattice MF results for the temperature dependence of η_s in Fig. 8(a). There are only some minor differences between Figs. 7(b) and 8(a):

For $H_1 = -2.9$ and $H_1 = -2.75$, the transition is discontinuous in the MF approximation. The reason is that the position of the tricritical line is slightly different.

The absolute value of η_s is in MF theory only half of the MC result. This can be attributed in part to the different values of the bulk OP's at T^*: $\eta_b^{MF} \simeq 0.55$, $\eta_b^{MC} \cong 0.75$. In addition, the mean distance of the interface from the surface is about 1.5 times larger in the simulations than in the MF result.

The behavior of the surface OP is particularly interesting. The temperature dependence of η_1 is shown in Fig. 7(c); the corresponding MF results are shown in Fig. 8(b). We first discuss the qualitative properties of η_1. The observed temperature dependence of η_1 can be described by an effective critical exponent $\beta_{1,\text{eff}}$. Figure 7(c) shows that $\beta_{1,\text{eff}}$ depends on the values of the surface fields: $\beta_{1,\text{eff}}$ increases with increasing distance of (H_1, H_2) from the tricritical line. However, for the two surface fields $(H_1, H_2) = (-2.75, -0.1375)$ and $(H_1, H_2) = (-2.9, -0.29)$, which are both on the tricritical line, we find the same (tricritical) exponent β_1'. $\beta_{1,\text{eff}}$ reaches an asymptotic value far away from the tricritical line, which is the true critical exponent β_1. The intermediate values of $\beta_{1,\text{eff}}$ are due to crossover effects. The crossover region is very broad: In order to see β_1 clearly, we have to choose surface fields so far away from the tricritical line that the A concentration in the surface exceeds $c_A = 0.75$. All these properties of the surface OP are also found in Fig. 8(b), the MF result; the remark concerning the position of the MF tricritical line made above applies here also.

From Fig. 7(c) we find

$$\beta_1 = 1.72 \pm 0.05 , \qquad \beta_1' = 0.81 \pm 0.05 .$$

Compared to the MF result $\beta_1^{(MF)} = 2.22$, the MC data yield a significantly smaller value for β_1. However, since the MF approximation indicates that β_1 depends on the ratio of two microscopic lengths in this case, this difference is not surprising. Nevertheless, we cannot exclude, *a priori*, the possibility that this discrepancy is due to capillary wave effects.

This can be tested by looking at the ratio of the critical

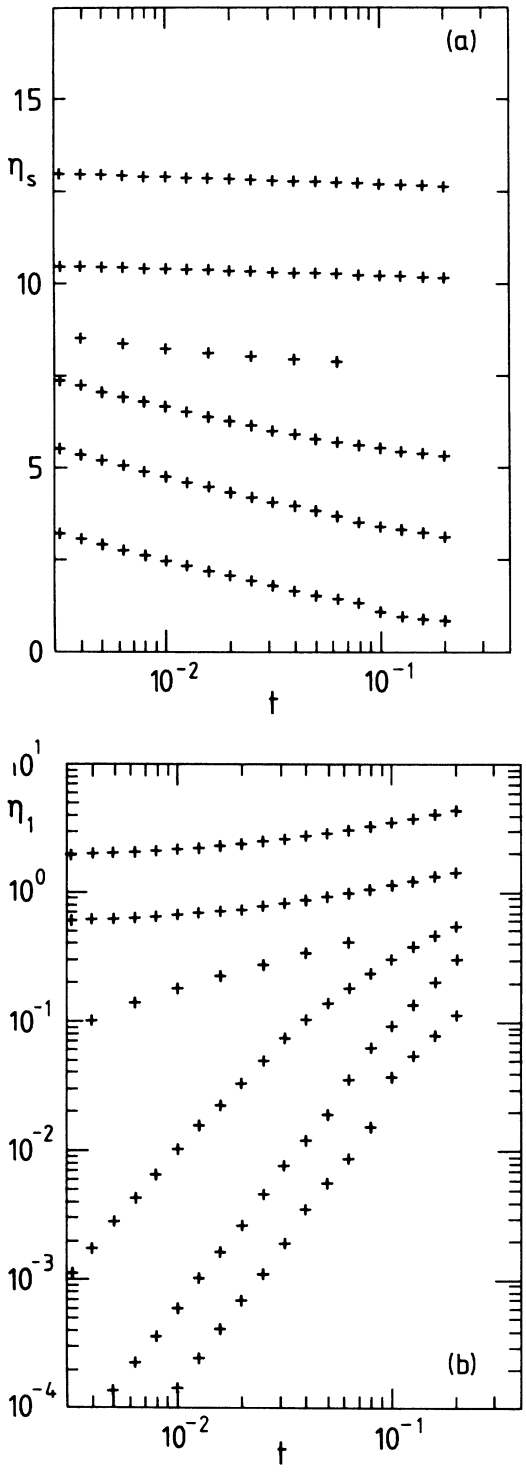

FIG. 8. Mean-field results for the surface excess order parameter η_s (a) and surface order parameter η_1 (b) for the (100) surface, plotted as a function of the reduced temperature t, for the same values of the surface fields and in the same presentation as the Monte Carlo data shown in Fig. 7.

and the tricritical surface exponent. The RG yields $\beta_1^t/\beta_1 > 0.5$ for all ω when $1 < \lambda_1/\lambda_2 = \beta_1^{(MF)} < 3$. For $\lambda_1/\lambda_2 > 3$ this ratio can be smaller; however, for the unique value of ω which yields $\beta_1 = 1.72$ in this case, one obtains $\beta_1^t/\beta_1 \simeq 0.58$. In contrast, the MC data give $\beta_1^t/\beta_1 \simeq 0.47 \pm 0.04$. The MC data are therefore consistent with the MF result $\beta_1^t/\beta_1 = \frac{1}{2}$ and give no indication of a fluctuation induced renormalization of the exponents. Note also that the linear dependence of η_1 on H_1 (at $t=0$) as the tricritical line is approached (see Figs. 3, 6, and 13) is consistent with the prediction of MF theory.

This observation is in agreement with the simulation results of Binder *et al.*[3] for wetting in the sc ferromagnetic Ising model: they also find that the critical behavior is consistent with simple (universal) MF behavior. The two simulations differ, however, in three important points.

(i) While Binder *et al.* are able to estimate the value of ω independently to be about $\omega = 1$, we have no information about ω whatsoever.

(ii) The location of the first-order bulk transition is known exactly in their model so that they can obtain more accurate values for the critical exponents.

(iii) Renormalized wetting exponents are expected only when the transition temperature is above the roughening temperature T_R of the system. Below T_R interface delocalization occurs by a series of layering transitions and is expected to show MF critical behavior (since $\omega = 0$). The simulation of Binder *et al.* is performed for temperatures above T_R. For our model, T_R is unknown. However, the absence of any signs of layering in the simulation data is an indication that $T^* > T_R$ in our model.

Order-parameter and concentration profiles near coexistence are shown in Fig. 9. Note that even for $t=0.01$, the distance of the kink position from the surface is rather small.

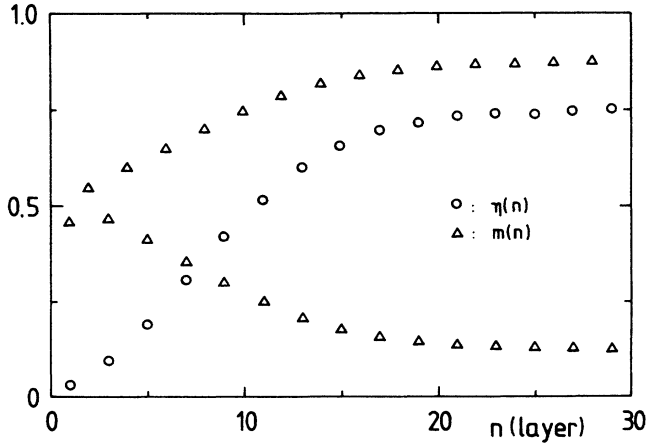

FIG. 9. Order parameter (○) and magnetization (△) profile in the (100) direction for $k_b T/J = 2.85$ and $H_1 = -2.5$, $H_2 = -0.12$.

3. *Surface magnetization*

Our data for the surface magnetization as a function of temperature for $H_1 = -2.0$ are compared with the MF result in Fig. 10(a). For this value of H_1, m_1 increases rather strongly as the transition temperature T^* is approached from below. In contrast, in the high temperature, disordered phase the temperature dependence is rather small. Near T^*, the magnetization is continuous, but decreases rapidly between T_L and T_U [T_L (T_U) is the temperature of the boundary between the ordered (disordered) and the two-phase region of the bulk phase diagram for $m = \frac{1}{2}$; see Fig. 10(b)].

As $T \to T_L^- = T^*$, the thickness $\langle z \rangle$ of the disordered surface phase diverges (i.e., becomes macroscopic). In the two-phase region $T_L < T < T_U$, $\langle z \rangle$ is determined by the condition that the total magnetization density of the

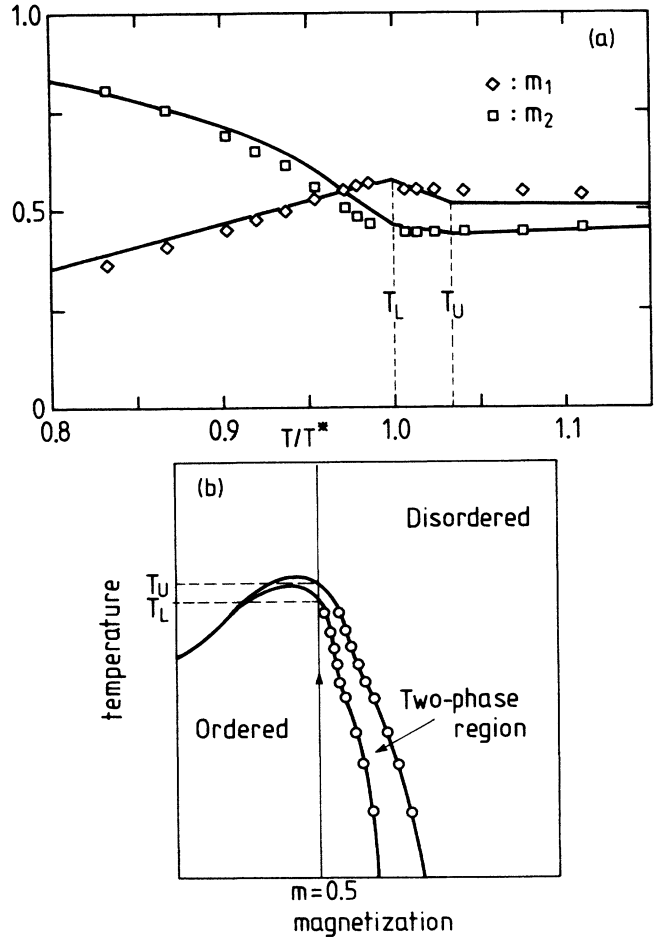

FIG. 10. (a) MF theory (solid lines) and MC simulation (◇,□) results for the surface magnetization as a function of temperature T, for $H_1 = -2.0$, $H_2 = -0.1$. The transition temperatures $T^* = T_L$ and T_U are $k_B T^*/J = 4.18$ and $k_B T_U/J = 4.32$ in the MF approximation, as indicated. For the MC data (with lattice size $L=24$, $D=30$) $k_B T^*/J = 2.88$ is used; the size of the two-phase region is smaller in this case. (b) Part of the bulk temperature-magnetization phase diagram of model (2.1) near $m=0.5$, obtained from MC simulations (Ref. 23).

sample is $\frac{1}{2}$. For $T > T_U$ the system is in the coherent disordered phase. The variation of the surface magnetization for $T_L < T < T_U$ reflects the (essentially) linear decrease of the bulk magnetization in the disordered phase as the two-phase region is transversed.

The size of variation of m_1 with temperature for $T < T_L$ depends rather sensitively on the values of H_1 and the surface enhancement. Indeed, for particular choices of these parameters the temperature dependence of m_1 can be substantially smaller.[16] At very low temperatures m_1 is approximately zero, independent of the value of H_1. For H_1 sufficiently negative, the surface magnetization remains small for all $T < T_L$. Decreasing H_1 therefore suppresses the temperature dependence of m_1 in the low-temperature phase. However, for the case considered here, in which the coupling constant in the surface, J_s, is equal to that in the bulk, the wetting transition becomes first order for $H_1 \lesssim -2.7$. For other choices of J_s, it should be possible to move the tricritical line to sufficiently negative values of H_1 so that we have a SID transition even when m_1 remains very small for all $T \leq T_L$. This would correspond to the observed behavior in Cu_3Au.[27]

4. Short-range order

In the bulk, short-range order (SRO) in the grand canonical ensemble is described by the correlation functions

$$g_b(\mathbf{r}) = \langle s_i s_j \rangle - m_b^2 ,$$

where $\mathbf{r}$ denotes the distance between the sites i,j on the lattice. This quantity is related to the standard Cowley short-range-order parameter $\alpha_b(\mathbf{r})$ by[11,12,28]

$$\alpha_b(\mathbf{r}) = g_b(\mathbf{r})/(1-m_b^2) .$$

Near a free surface, the short-range order will not only depend on the distance between the lattice sites, but also on their distances from the surface. Therefore, we define the SRO parameters $\alpha_n(\mathbf{r})$ for spins i,j, which are both in layer n:

$$\alpha_n(\mathbf{r}) = [\langle s_i^{(n)} s_j^{(n)} \rangle - m_n^2]/(1-m_n^2) .$$

A generalization for spins in different layers is straightforward but will not be considered here.

The data for $\alpha_1(\mathbf{r})$ and $\alpha_2(\mathbf{r})$ are presented in Figs. 11 and 12 for surface fields which lead to a second- and first-order transition, respectively. Due to the antiferromagnetic coupling, $\alpha_1(\mathbf{r})$ is negative if $\mathbf{r}$ is a nearest-neighbor distance. $|\alpha_1(\mathbf{r})|$ is found to decrease as a function of distance and as a function of temperature—just as expected. On the other hand, $\alpha_2(\mathbf{r})$ shows a very unusual behavior, which is directly related to the highly interlocked structure of the fcc lattice: Below the bulk transition temperature, an antiferromagnetic structure appears in the short-range correlations which increases with temperature. Above T^*, it decreases again, paralleling the decrease of the order in the whole lattice.

For $H_1 = -3.5$, α_2 has a clear jump at $T = T^*$, while the jump of α_1 is too small to be seen. The data for $H_1 = -2.0$ are continuous as a function of temperature.

5. α Dependence of the critical exponents

In the MF approximation, β_1 was found to depend on the ratio α of NN and NNN couplings. For example, $\beta_1 = 2.8$ for $\alpha = 0.1$, $\beta_1 = 2.2$ for $\alpha = 0.2$, and $\beta_1 = 1.9$ for $\alpha = 0.3$. Since the bulk phase diagram changes its topology near $\alpha = 0.25$, we have determined β_1 for $\alpha = 0.1$ in order to compare with the $\alpha = 0.2$ results of the last paragraph.

In order to calculate β_1 and β_1' for $\alpha = 0.1$, we have to first determine the position of the tricritical line. Data for $\eta_1(H_1)$ at coexistence, with H_2/H_1 fixed, are shown in Fig. 13. By linear extrapolation of the data for

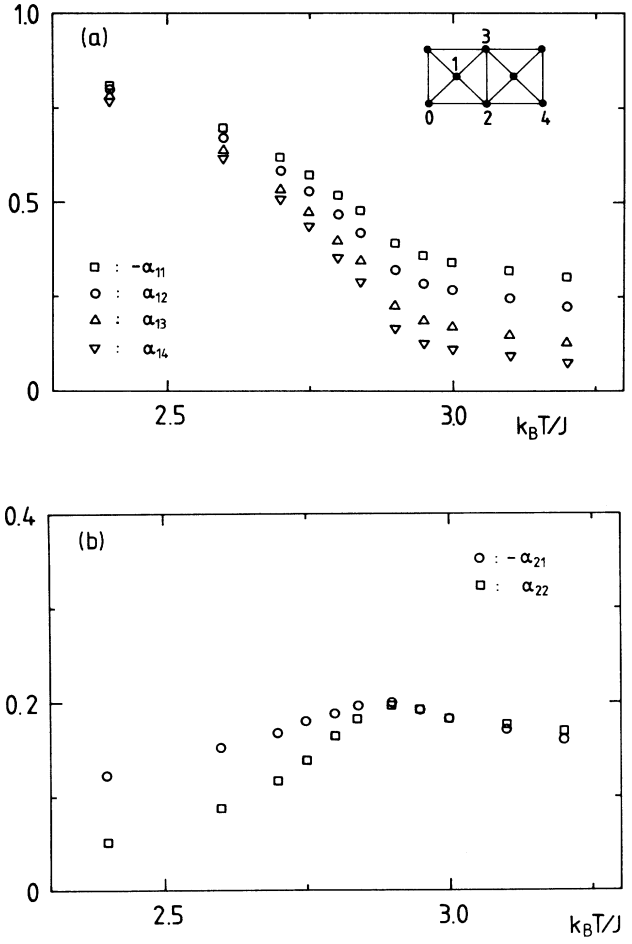

FIG. 11. Short-range-order parameters α_{ij} for $H_1 = -2.0$, $H_2 = -0.1$, where the surface transition is continuous, as a function of temperature T. Data for the first ($i=1$) and the second ($i=2$) layer are given in part (a) and (b) of the figure, respectively, for nearest (α_{i1}), next-nearest- (α_{i2}), third- (α_{i3}), and fifth- (α_{i4}) nearest-neighbor distances, as shown by the inset in (a). Lattice size is $L=24$, $D=30$.

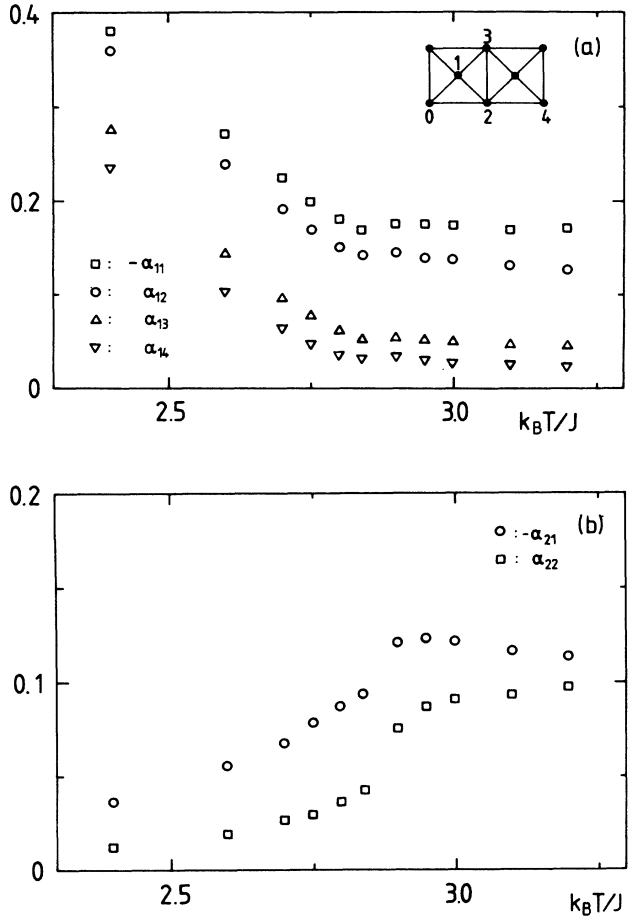

FIG. 12. Short-range-order parameters α_{ij} for $H_1=-3.5$, $H_2=0$, where the surface transition is discontinuous, as a function of temperature T. Data for the first ($i=1$) and the second ($i=2$) layer are given in part (a) and (b) of the figure, respectively, for nearest (α_{i1}), next-nearest- (α_{i2}), third- (α_{i3}), and fifth- (α_{i4}) nearest-neighbor distances, as shown by the inset in (a). Lattice size is $L=24$, $D=30$.

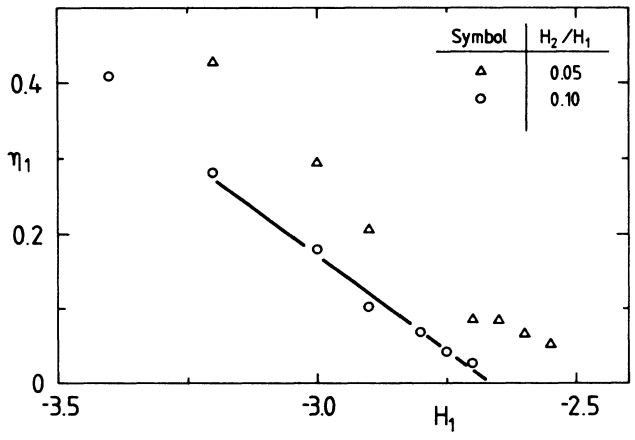

FIG. 13. Surface order parameter η_1 for $\alpha=0.1$ at coexistence ($k_BT/J=2.340$), as a function of the surface field H_1 and for two values of H_2/H_1 as indicated; lattice size $L=40$, $D=46$.

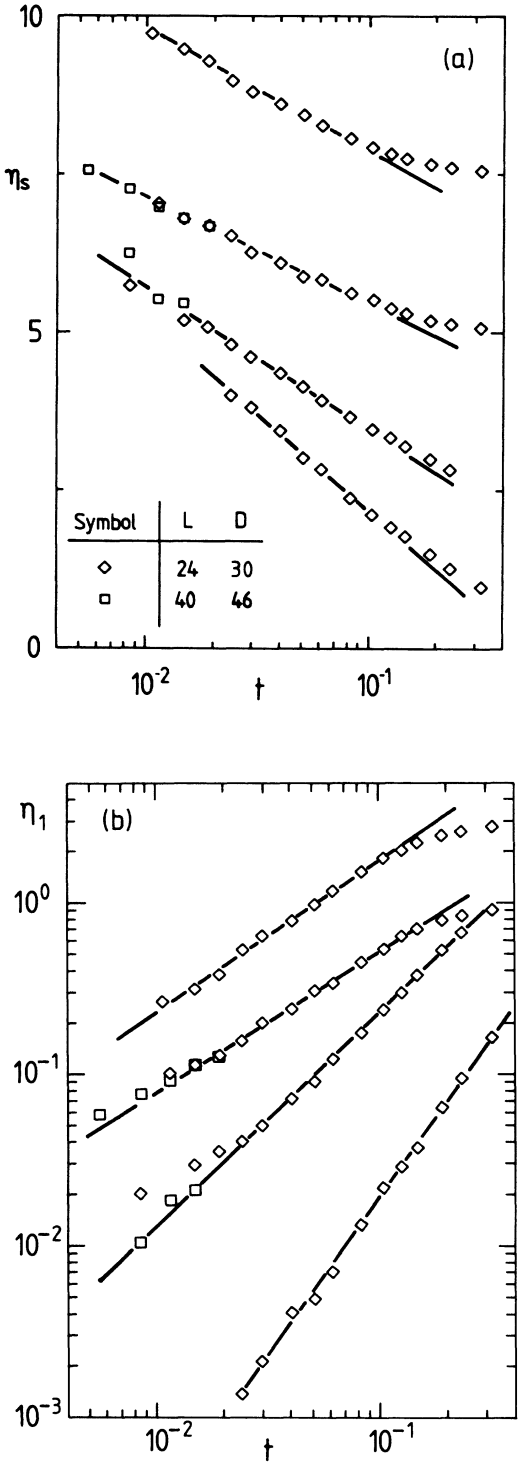

FIG. 14. Surface excess order parameter η_s (a) and surface order parameter η_1 (b) for the (100) surface with $\alpha=0.1$, plotted as a function of the reduced temperature t (with $k_BT^*/J=2.345$) for several values of the surface fields (Ref. 29). Data shown are (from bottom to top) for $H_1=-1.0$, $H_2=-0.2$, for $H_1=-2.0$, $H_2=-0.1$, for $H_1=-2.5$, $H_2=-0.12$, and for $H_1=-2.67$, $H_2=-0.267$. In (a), data for successive values of the fields are incremented by 2.5 to separate them in the figure. In (b), the data for $H_1=-2.67$ are multiplied by a factor of 3. The solid lines are an approximate fit to the asymptotic slope of the data.

$H_2/H_1=0.1$, we obtain the tricritical point $(H_1,H_2)=(-2.67,-0.267)$. The temperature dependence of η_s and η_1 is presented in Fig. 14 for several surface fields corresponding to various distances form the tricritical line. As before, the surface excess OP shows the expected logarithmic behavior for reduced temperatures smaller than $t\cong 0.1$. Figure 14(b) yields the desired critical exponents

$$\beta_1^t=0.88\pm 0.05\ ,$$

$$\beta_1=1.84\pm 0.05\ .$$

Decreasing α therefore leads to an increase in β_1 and β_1^t, just as in the MF approximation. Note however that the relative increase is substantially smaller than that predicted by MF theory.

B. (111) surface

The SID transition at the (111) surface is found to be continuous for *all* surface fields H_1.[30] This can be understood in the following way. Assume that H_1 is chosen so that we have the stoichiometric composition at the sur-

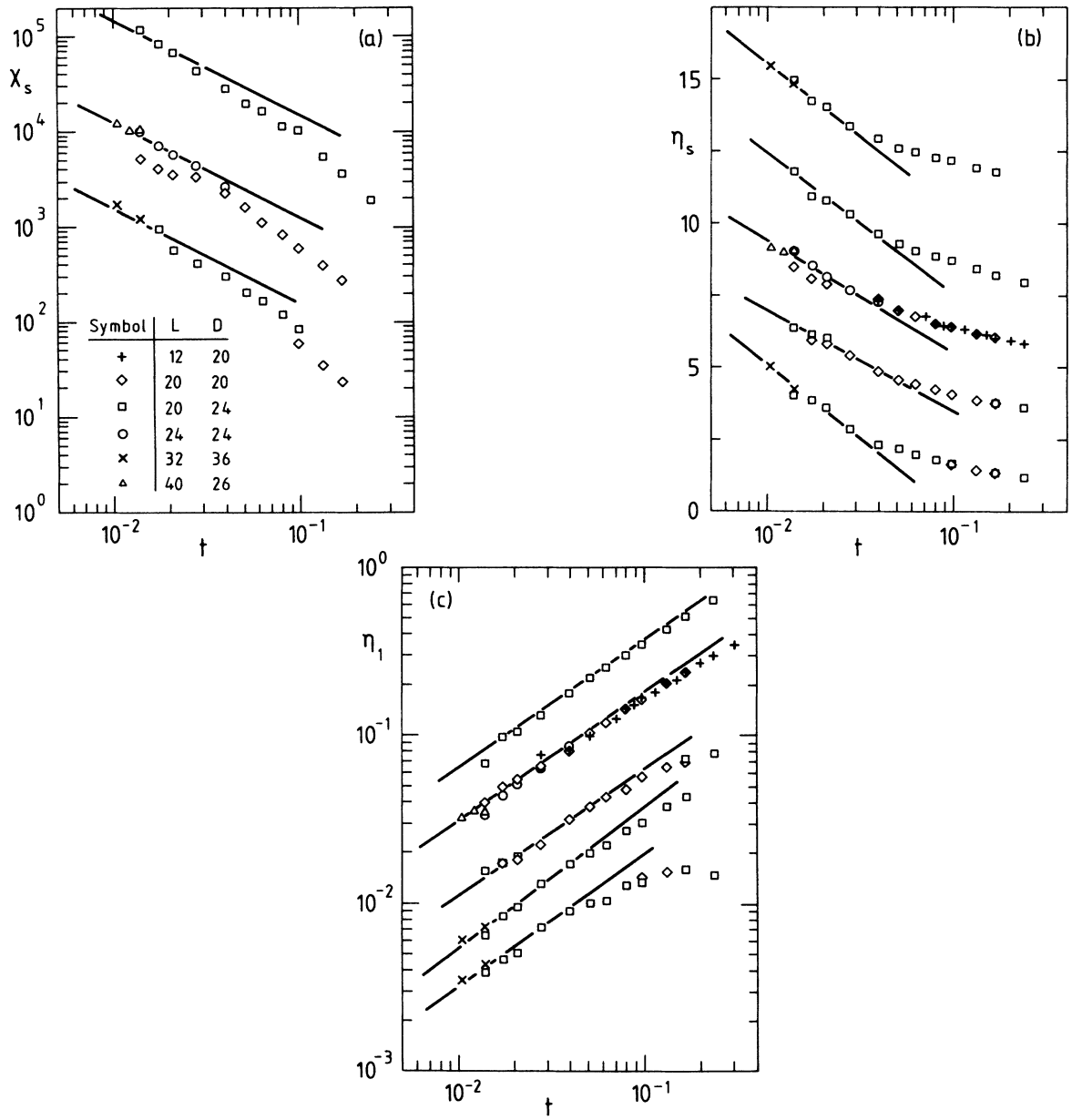

FIG. 15. Surface excess susceptibility χ_s (a), surface excess order parameter η_s (b), and surface order parameter η_1 (c) for the (111) surface, plotted as a function of the reduced temperature t (with $k_BT^*/J=2.880$) for several values of the surface fields. In (a), data (from bottom to top) for $H_1=-1$, for $H_1=0$, and for $H_1=-5$ are shown. Data for successive values of the fields are multiplied by a factor of 10 to separate them in the figure. In (b), data (from bottom to top) for $H_1=4$, for $H_1=2$, for $H_1=0$, for $H_1=-5$, and for $H_1=-12$ are shown. Data for successive values of the fields are incremented by 2.5 to separate them in the figure. In (c), data (from bottom to top) for $H_1=4$, for $H_1=-12$, for $H_1=2$, for $H_1=0$, and for $H_1=-5$ are shown. The data for $H_1=-12$ are multiplied by a factor of 0.5. The solid lines are an approximate fit to the asymptotic slope of the data.

face. If the effect of the missing neighbors at the surface is sufficient for a continuous transition—this depends on the surface enhancement—then the transition is continuous for all surface fields, since deviations from stoichiometry enhance the surface disorder. We expect from this argument that the surface OP is largest for those surface fields which lead to the stoichiometric surface composition.

Figures 15(a) and 15(b) show the critical temperature dependence of the excess OP η_s and the surface excess susceptibility χ_s for several values of H_1. The data exhibit the expected scaling behavior [Eq. (4.5)] for $t \lesssim 0.05$. The width of the asymptotic scaling regime is thus about the same as at the (100) surface. In addition, we again find that the value of η_s is about a factor of 2 greater than that predicted by MF theory [see Fig. 16(a) and the discussion following Eq. (4.5)].

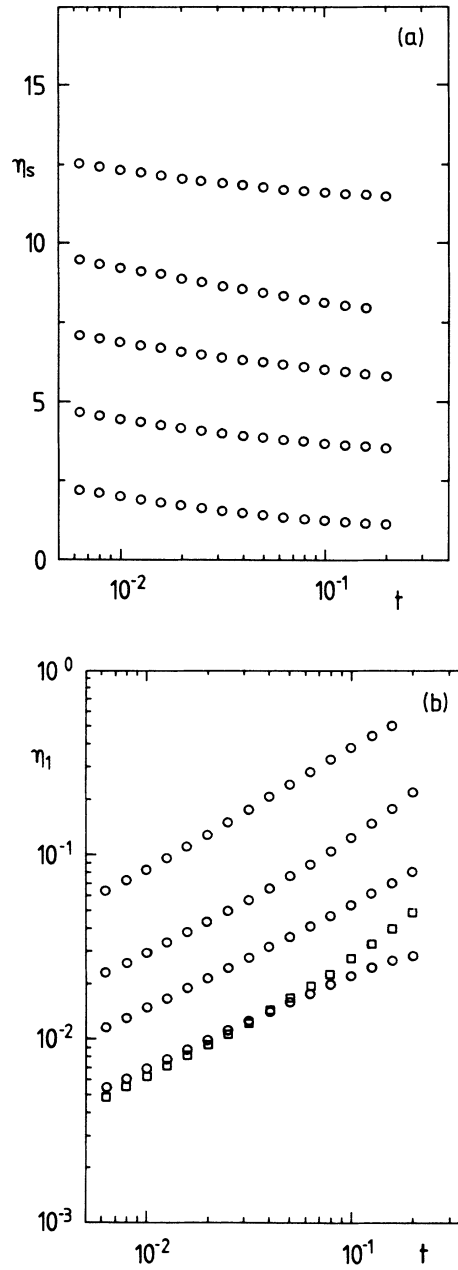

FIG. 16. Mean-field results for the surface excess order parameter η_s (a) and surface order parameter η_1 (b) for the (111) surface, plotted as a function of the reduced temperature t for the same values of the surface fields and in the same presentation as the Monte Carlo data shown in Fig. 15.

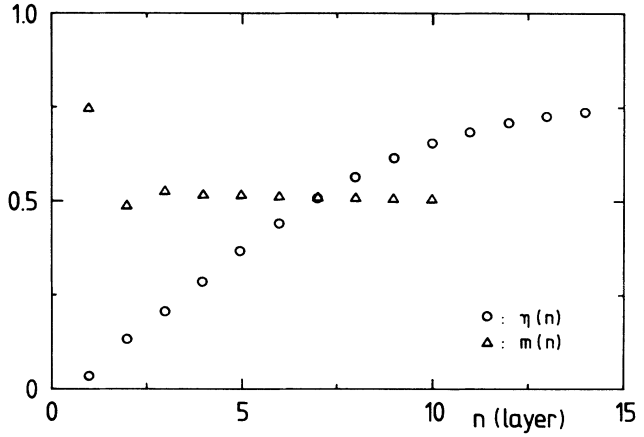

FIG. 17. Order parameter (○) and magnetization (△) profile in the (111) direction for $k_B T/J = 2.84$ and $H_1 = 0$.

In Fig. 15(c) we have plotted the critical temperature dependence of η_1 for several surface fields. Since MF theory predicts a universal exponent $\beta_1^{(MF)} = 0.5$, it is much easier than at the (100) surface to distinguish between MF and RG behavior. Inspection of the slopes in Fig. 15(c) gives values for β_1 (depending on the surface field) which are all larger than $\beta_1^{(MF)}$. However, the deviations from the MF value are rather small, and, furthermore, the MF results shown in Fig. 16(b) also have slopes slightly greater than 0.5 in this range of reduced temperatures. The scatter of the data is too large for these small deviations to be significant. We therefore conclude again that the MC data are consistent with the predictions of MF theory.

Finally, Fig. 17 shows the order parameter and magnetization profiles. As for the (100) surface, the interface is very near the surface. Even for the smallest values of the reduced temperature considered, the profiles are just beginning to show the characteristic kink shape.

V. CONCLUSIONS

We have given a detailed description of the surface phase diagram, the critical behavior of both excess and local surface quantities, as well as the behavior of the short-range-order parameter at the surface at the order-disorder transition in an fcc Ising antiferromagnet with NN and NNN interactions which exhibits a $L1_2$ (A_3B) ground-state structure. While it is known that the MF predictions for the bulk phase diagram of this model are *qualitatively* wrong,[12] we find that it does an excellent job of describing the behavior at SID transitions. In fact, several predictions are in quantitative agreement with our data; in particular, the wetting critical behavior was

found to be consistent with the predictions of MF theory.

Needless to say, we have only considered a very simple model. Although it may correctly describe many properties of a magnetic insulator (with short-range interactions), it is not expected to faithfully represent any real alloy system or magnet with indirect or itinerate exchange. For example, in the rare earths, strongly localized f electrons polarize the conduction electrons and induce, in this way, oscillatory, long-range RKKY interactions. The interactions in ordering alloys such as Cu_3Au are of similar form.[11]

While the qualitative features of the wetting phase diagram of the present model should also apply to ordering alloys, certain details, such as the values of the critical exponents or the nonuniversal critical behavior we find at (100) surfaces, are intimately connected with the short-range nature of the interactions; the nonuniversal behavior is a feature of wetting when the dimensionality of the OP is greater than 1 in this case.

In general, the wetting exponents depend rather sensitively on the range and type of interaction.[31,32] Because of this, measurements of the surface OP or the coverage, characterized by the behavior of z^*, at SID transitions, would provide a useful test of our understanding of magnetic or ordering interactions in these systems. This would be very important since the interaction parameters in real materials are in general not well known.

While LEED (Ref. 33) or SPLEED (Ref. 34) yields information about local surface quantities, a total reflection experiment[35,36] allows a direct determination of z^*. X-rays or neutrons can be rendered surface sensitive by total reflection: for angles of incidence α_i smaller than the critical angle α_c of total reflection, the incoming wave decays exponentially into the bulk of the material (on the length scale of the penetration depth, l). For temperatures sufficiently close to the transition, the interface width is generally small compared to both the penetration depth and the thickness of the disordered surface phase. In this case, the intensity I_B of the superlattice Bragg peak decays exponentially with z^*: $I_B \sim \exp(-2z^*/l)$.[36,37] For short-range interactions, $z^* = z_0 \cdot \ln(t)$, so that $I_B \sim t^{\beta_B}$, with $\beta_B = 2z_0/l$. As an example, consider the parameter values appropriate for Cu_3Au, $a_0 = 1.87$ Å and minimal penetration depth $l_0 = 30$ Å.[35] From the simulation data we obtain $z_0 \cong 2a_0$ for the (100) surface. This yields $\beta_B = 0.4$ for $\alpha_i = \alpha_f = \alpha_c/2$, and $\beta_B = 0.2$ for $\alpha_i = \alpha_c/2$, $\alpha_f \geq \alpha_c$ (where α_f denotes the exit angle of the scattered radiation). Thus, the Bragg intensity drops about 1 order of magnitude over the temperature range $0.001 \leq t \leq 0.1$.

Finally, throughout our discussion we have assumed that the system has attained thermodynamic equilibrium. This may not be the case in experiments on ordering alloys. The wetting phenomena we considered occurs when the system approaches the order-disorder transition from the low-temperature, ordered phase [see Fig. 10(b)]. The concentration in the disordered phase which forms at the crystal surface is different from that in the ordered bulk. Equilibrium therefore requires the transfer of atoms over length scales of the order of the wetting layer thickness; this is clearly not possible on the time scale of a typical experiment. This fact has several consequences. First, the measured temperature dependence of the concentration in the surface layer, c_1, may be substantially smaller in the low-temperature phase than predicted by theory. However, as noted in Sec. IV A 3, similar behavior is expected for certain choices of H_1 and surface enhancement. In a given experiment, it may be difficult to decide which of these two possibilities is the real cause of such behavior.[27,33,34] Second, it is not *a priori* obvious that this effect will not influence the values of the critical exponents, or at least the nonuniversal behavior which occurs at (100) surfaces in the present model. The MF results discussed in Ref. 10 indicate, however, that this should not be the case. Consider first the [111] direction. Two densities are needed to describe the wetting behavior in this case. However, the length scale of the concentration mode is very short; as a consequence it can be shown that the universal features of the surface critical behavior will not be influenced by the details of the concentration profile. In the [100] direction three densities are needed to describe the wetting profiles. Two of these, the order parameter and the difference in concentration between adjacent planes, have correlation lengths of comparable size; they couple strongly to cause the characteristic nonuniversal behavior discussed above. Also, equilibration is fast because it requires only a local redistribution of atoms. The third mode, the average concentration density in neighboring planes, equilibrates slowly. However, it has only a very short correlation length so that, just as in the [111] direction, we do not expect this fact to influence the essential features of the nonuniversal critical behavior.

ACKNOWLEDGMENTS

We thank K. Binder, S. Dietrich, R. Lipowsky, and H. Wagner for many stimulating discussions. The hospitality of the Institut für Festkörperphysik der KFA Jülich, and of the Institut für Theoretische Physik der Ludwig-Maximilians-Universität München during mutual visits, are gratefully acknowledged.

[1]For a recent review and an extensive list of references, see S. Dietrich, in *Phase Transitions and Critical Phenomena, Vol. 12*, edited by C. Domb and J. Lebowitz (Academic, New York, 1988).

[2]D. M. Kroll, J. Appl. Phys. **61**, 3595 (1987).

[3]K. Binder, D. P. Landau, and D. M. Kroll, Phys. Rev. Lett. **56**, 2272 (1986).

[4]R. Lipowsky, D. M. Kroll, and R. K. P. Zia, Phys. Rev. B **27**, 4499 (1983).

[5]E. Brézin, B. I. Halperin, and S. Leibler, Phys. Rev. Lett. **50**,

1387 (1983).
[6]D. S. Fisher and D. A. Huse, Phys. Rev. B **32**, 247 (1985).
[7]R. Lipowsky and M. E. Fisher, Phys. Rev. Lett. **57**, 2411 (1986); Phys. Rev. B **36**, 2126 (1987).
[8]G. Gompper and D. M. Kroll, Phys. Rev. B **37**, 3821 (1988).
[9]R. Lipowsky, Phys. Rev. Lett. **49**, 1575 (1982); J. Appl. Phys. **55**, 2485 (1984).
[10]D. M. Kroll and G. Gompper, Phys. Rev. B **36**, 7078 (1987).
[11]For a review and general references see D. Fontaine in *Solid State Physics,* edited by H. Ehrenreich, F. Seitz, and D. Turnbull (Academic, New York, 1979), Vol. 34.
[12]K. Binder, in *Festkörperprobleme-Advances in Solid State Physics,* edited by P. Grosse (Vieweg, Braunschweig, 1986), Vol. 26.
[13]The relation of our work to other MF treatments (Refs. 14–16) of surface effects in fcc Ising antiferromagnets, as well as the discrepancies, are discussed in Ref. 1.
[14]V. Kumar and K. H. Bennemann, Phys. Rev. Lett. **53**, 278 (1984).
[15]J. L. Morán-López, F. Mejíra-Lira, and K. H. Bennemann, Phys. Rev. Lett. **54**, 1936 (1985); F. Mejíra-Lira, K. H. Bennemann, and J. L. Morán-López, Phys. Rev. B **32**, 5926 (1985).
[16]J. M. Sanchez and J. L. Morán-López, Surf. Sci. **157**, L297 (1985); Phys. Rev. B **32**, 3534 (1985).
[17]E. H. Hauge (Ref. 18) has obtained many of these results independently.
[18]E. H. Hauge, Phys. Rev. B **33**, 3322 (1986).
[19]R. Lipowsky, Ferroelectrics **73**, 69 (1987).
[20]E. Brézin and T. Halpin-Healy, J. Phys. (Paris) **408**, 775 (1987).
[21]The renormalization of an effective interface model with two different length scales has also been discussed by E. H. Hauge and K. Olaussen, Phys. Rev. B **32**, 4766 (1985).
[22]K. Binder, J. L. Lebowitz, M. K. Phani, and M. H. Kalos, Acta Metall. **29**, 1655 (1981).
[23]K. Binder, W. Kinzel, and W. Selke, J. Magn. Mag. Mater. **31-34**, 1445 (1983).
[24]We assume that the coefficients of the higher-order terms in (2.2) are positive. Our MC data indicate that $\frac{3}{2}\lambda_2 < \lambda_1 < 2\lambda_2$ (see Sec. IV A 2) so that the three leading terms in (2.2) are powers of $e^{-\lambda_2 z}$.
[25]Other scenarios are also possible; for example, if B_2 remains positive and C_2 changes sign. Since we do not have enough data to distinguish between the various possibilities, we present here only the simplest scenario which is consistent with our data. For a discussion of other possibilities see Ref. 32.
[26]In Fig. 7 we use the value $k_B T^*/J = 2.88$ for the transition temperature instead of $k_B T^*/J = 2.87$ as in the preceeding figures, since scaling seems to be slightly better in this case. Note, however, that for the range of reduced temperatures and surface fields used in the MC simulations, both values of T^* are essentially equivalent.
[27]T. M. Buck, G. H. Wheatley, and L. Marchut, Phys. Rev. Lett. **51**, 43 (1983).
[28]J. M. Cowley, Phys. Rev. **77**, 669 (1950).
[29]The difference in values for the temperatures at coexistence used in Figs. 13 and 14 is less than the uncertainty in T^*.
[30]There is an additional field H_1 only on the surface plane at (111) surfaces (see Ref. 10).
[31]S. Dietrich and M. Schick, Phys. Rev. B **31**, 392 (1985).
[32]C. Ebner, W. F. Saam, and A. K. Sen, Phys. Rev. B **31**, 6134 (1985).
[33]E. G. McRae and R. A. Malic, Surf. Sci. **148**, 551 (1984).
[34]S. F. Alvarado, M. Campagna, A. Fattah, and W. Uelhoff, Z. Phys. B **66**, 103 (1987).
[35]S. Dietrich and H. Wagner, Phys. Rev. Lett. **51**, 1469 (1983); Z. Phys. B **56**, 207 (1984).
[36]N. Bernhad, E. Burkel, G. Gompper, H. Metzger, J. Peisl, H. Wagner, and G. Wallner, Z. Phys. B **69**, 303 (1987).
[37]For $\lambda_1 \ll 1/l$, $I_B \sim \exp(-2\lambda_1 z^*)$. In this limit total reflection can be used to determine β_1.